Differential cross sections and analyzing powers for *pp* elastic scattering at 1.46 GeV/*c* in the Coulomb-nuclear interference region

G. Pauletta, G. Adams,* S. M. Haji-saeid, G. J. Igo, J. B. McClelland,†
A. T. M. Wang, C. A. Whitten, Jr., and A. Wriekat‡
University of California, Los Angeles, California 90024

M. M. Gazzaly
University of Minnesota, Minneapolis, Minnesota 55455

N. Tanaka
Los Alamos National Laboratory, Los Alamos, New Mexico 87545
(Received 9 July 1982)

Differential cross sections $\sigma(\theta)$ and analyzing powers $A(\theta)$ for *pp* elastic scattering have been measured in the Coulomb-nuclear interference region at 800 MeV. The measurements, which extend down to 0.5 deg in the laboratory, have been analyzed to deduce the zero-degree *pp* scattering amplitudes. The ratio ρ of the real to imaginary parts of the spin-independent amplitude was found to be -0.04 ± 0.04; the contribution of the double-spin-flip amplitudes to $\sigma(0)$ was found to be 0.16 ± 0.03 times that of the spin-independent amplitude; while the ratios of the imaginary and real parts of the single spin-flip amplitude to $\sin\theta$ were found to be 0.74 ± 0.04 and -0.03 ± 0.08 fm, respectively. Except for the last, these experimental values agree with the predictions of forward dispersion relations and phase shift analyses.

[NUCLEAR REACTIONS ^{1}H$(p,p)^1$H, $E=800$ MeV, measured $\sigma(\theta)$ and $A(\theta)$. Deduced zero-degree scattering amplitudes.]

I. INTRODUCTION

The measurement of *pp* elastic scattering observables in the Coulomb-nuclear interference region is an effective means of unravelling the various components of the *pp* scattering amplitude. The reason for this is that the interference between the nuclear and the well-known electromagnetic (em) components of the amplitude result in terms which are linear in the nuclear parts. (This is to be contrasted with the situation outside of the interference region where all observables are bilinear in the nuclear parts.) These interference terms make the phases of the nuclear components accessible.

The *pp* scattering amplitude may be parametrized as follows[1]:

$$M=\alpha+i\gamma(\vec{\sigma}_1+\vec{\sigma}_2)\cdot\hat{n}+\beta(\vec{\sigma}_1\cdot\hat{n})(\vec{\sigma}_2\cdot\hat{n}) +\delta(\vec{\sigma}_1\cdot\hat{s})(\vec{\sigma}_2\cdot\hat{s})+\epsilon(\vec{\sigma}_1\cdot\hat{l})(\vec{\sigma}_2\cdot\hat{l})\ . \quad (1.1)$$

The amplitudes α, γ, β, δ, and ϵ are complex functions of the center-of-mass (c.m.) energy E and of the c.m. scattering angle θ. The orthogonal set of unit vectors is defined by:

$$\hat{n}=(\vec{p}_i\times\vec{p}_f)/(\,|\,\vec{p}_i\times\vec{p}_f\,|\,)\ ,$$
$$\hat{s}=(\vec{p}_f-\vec{p}_i)/(\,|\,\vec{p}_f-\vec{p}_i\,|\,)\ , \quad (1.2)$$
$$\hat{l}=(\hat{p}_i+\vec{p}_f)/(\,|\,\vec{p}_i+\vec{p}_f\,|\,)\ ,$$

where $\vec{p}_i$ is the c.m. momentum of the incident proton and $\vec{p}_f$ is that of the scattered proton so that $p_i=p_f=p$. Total angular momentum conservation implies that $\gamma(0)=0$ and $\beta(0)=\delta(0)$. The imaginary parts of $\alpha(0)$, $\beta(0)$, and $\epsilon(0)$ may be determined from total cross section measurements by the generalized optical theorem,[1] i.e.,

$$\mathrm{Im}\alpha(0)=(p/4\pi\hbar)\sigma_{\mathrm{tot}}\ ,$$
$$\mathrm{Im}\beta(0)=(p/8\pi\hbar)\Delta\sigma_T\ , \quad (1.3)$$
$$\mathrm{Im}\epsilon(0)=(p/4\pi\hbar)\Delta\sigma_l\ ,$$

where σ_{tot} is the spin-averaged total cross section, while $\Delta\sigma_T$ and $\Delta\sigma_l$ are the asymmetries in the total cross section in the pure transverse and longitudinal spin states, respectively.[1]

These experimentally determined imaginary amplitudes may be used as input to forward dispersion

relations (FDR) calculations in order to calculate the corresponding real parts.[2] However, since these calculations require data spanning a large interval of incident energy and incorporate certain model-dependent assumptions,[2] it is important to verify them experimentally, particularly at intermediate energies because of their relevance to speculations concerning the existence of dibaryon resonances.[2] Although empirical verification of $\mathrm{Re}\epsilon(0)$ and of $\mathrm{Re}\beta(0)$ are particularly relevant to these speculations, it was pointed out by Hoshizaki[3] that the energy dependence of $\rho=\mathrm{Re}\alpha(0)/\mathrm{Im}\alpha(0)$ near 800 MeV is also characteristic of resonance structure.

By measuring the spin-averaged differential cross section $\sigma(\theta)$ in the Coulomb-nuclear interference region, ρ may be determined, either from phase shift analysis, or by more direct analysis (see Sec. V). From the same data (assuming $\gamma=0$) one can also extract

$$S(0)=2\,|\beta(0)|^2+|\epsilon(0)|^2$$

(Ref. 4). However, γ contributes significantly to $\sigma(\theta)$ over part of the angular range considered, i.e., for $\theta \gtrsim 5°$, so that the assumption $\gamma=0$ severely limits the accuracy with which S may be determined. This limitation may be eliminated by measuring the analyzing power $A(\theta)$ in the Coulomb interference region, from which one can determine $\mathrm{Re}\gamma$ and $\mathrm{Im}\gamma$ in the region of interest (see Sec. V). One can then make a more significant comparison between the empirical value of S and the predictions of the FDR calculations. Of course, it would be preferable for individual values of $\mathrm{Re}\beta(0)$ and $\mathrm{Re}\epsilon(0)$ to be the subject of comparison. However, to determine these empirically, one must measure spin-correlation parameters in the Coulomb-nuclear interference region. This is a difficult experiment which has not yet been attempted.

Apart from the above considerations, empirical determination of $\mathrm{Re}\gamma$ and $\mathrm{Im}\gamma$ at forward angles has intrinsic value and would also introduce an important constraint on the microscopic analysis[5] of p-nucleus scattering data at intermediate energies.

Differential elastic cross sections for pp scattering in the Coulomb-nuclear interference region have already been measured at energies close to the one reported here.[6–8] However, they are too inaccurate to afford significant comparison with theory. A pronounced discrepancy also exists between the data of Dutton *et al.*[6,7] and those of Vorobyov *et al.*[8] Neither of these measurements includes analyzing powers. At lower energies analyzing powers were measured by Besset *et al.*[9] and by Aebischer *et al.*[10] At 800 MeV, a measurement was performed at LAMPF, concurrently with the work reported here.[11] However, these data do not extend far enough into the interference region to determine γ completely. The accuracy of these data is, however, comparable to that of the data reported here and they therefore afford a valuable comparison.

In this paper, measurements of both $\sigma(\theta)$ and $A(\theta)$ are reported. The measurements were extended to much smaller angles ($\theta_{\mathrm{lab}}=0.5°$) than any previously reported and permitted both $\mathrm{Re}\gamma$ and $\mathrm{Im}\gamma$ to be determined at small angles.

The experiment is described in Sec. II and the data reduction in Sec. III. The results are presented in Sec. IV. In Sec. V the analysis is described and, finally, in Sec. VI, the results are discussed.

II. EXPERIMENTAL METHOD

The experiment was performed at the Los Alamos Meson Physics Facility (LAMPF) using the high resolution spectrometer (HRS).[12] Data were taken in two stages. The differential elastic cross section, $\sigma(\theta)$, was first measured using an 800 MeV unpolarized proton beam. A brief description of the experiment has already been published.[4] The experiment was repeated a year later with the polarized proton beam. Both differential cross sections and analyzing powers $A(\theta)$ were measured. In this section the experimental method will be described, with emphasis on those aspects relevant to the measurement of analyzing powers.

A. Beam transport

The HRS beam line is characterized by good beam stability, small emittance, and good phase-space control. The experiment was designed to take advantage of these qualities in order to extend measurements to very small angles with good resolution. Figure 1 shows part of the LAMPF proton beam transport. Only those elements relevant to this ex-

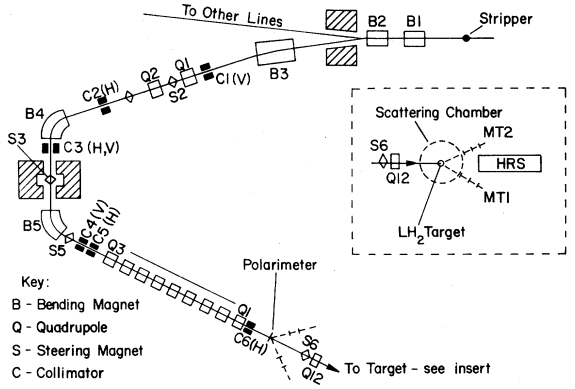

FIG. 1. HRS beam line and spectrometer. The arrangement of the monitor telescopes ($MT1$ and $MT2$) about the target is also shown.

periment are shown. The phase space of the negatively ionized proton beam is controlled primarily by means of a set of strippers (not shown in Fig. 1) situated some distance upstream of the beam split. The fraction of the residual beam required is stripped by means of foil strippers of variable thickness situated in front of the beam split. The resulting proton beam is deflected into the HRS line where its momentum dispersion is increased (by bending magnets $B4$ and $B5$) and rotated through 90° (by quadrupole magnets $Q3$—$Q9$) for dispersion matching with HRS.[12] The beam may be further tailored by means of a set of collimators $C1$—$C7$. The beam line was first tuned with an uncollimated beam. The upstream strippers were then closed down to select a small fraction of the total phase space. The intensity of the resulting "pencil beam" was then reduced to $\lesssim 10^5$ proton/sec and the spectrometer was moved to 0°. In this configuration, the beam profile could be monitored on the focal plane detectors. All collimators ($C1$—$C7$) were then closed tightly around the beam in order to prevent the beam from drifting on target. A stable beam spot 1 mm wide and 2 mm high, with a horizontal divergence (FWHM) of 0.5 mrad and a vertical one of 3.4 mrad, was obtained.

B. Beam polarization monitors

The polarimeter in our line[13] (see Fig. 1), comprising a CH_2 target of variable thickness and left-right scintillator telescopes, could not be used because of the low beam intensity used in this experiment. Multiple Coulomb scattering from a polarimeter target of sufficient thickness to obtain an adequate count rate in the polarimeter counters would also have increased the beam divergence, and therefore the angular resolution, beyond tolerable values. Therefore the polarization of that part of the beam which proceeds unstripped into another line (see Fig. 1) was monitored continuously by a similar polarimeter[13] in that line. It has been verified that the variation in polarization as a function of phase space is small ($<5\%$). The beam polarization at the source was also monitored periodically by the "quench ratio" method.[14,15] The result of these measurements agreed with those of the polarimeter to within 5%. The average beam polarization was $\sim 81\%$. Its direction was reversed every 60 sec.

C. Targets

The LH_2 target was constructed by the LAMPF cryogenic group. The target cell, constructed from 0.13 mm kaptan, was a cylinder, 6 cm in length, mounted so that its axis coincided with that of the beam. A 5 mm-thick CH_2 target and a number of wire targets were mounted below it. The target assembly could be moved vertically so as to position any target at beam level. The CH_2 target was used to determine the absolute cross section as described in Ref. 4 while the wire targets were needed for calibration purposes (see Sec. II D). During the second stage of the experiment, a cell identical with the one containing LH_2 was mounted below the LH_2 target. This "dummy target" was used to measure target-associated background and, thereby, to extend the measurements to momentum transfers where the events due to scattering off hydrogen could not be distinguished from those due to scattering off the target walls (see Sec. III).

D. Focal plane detectors

The detector assembly at the focal plane of the HRS is shown schematically in Fig. 2. Scintillation counters $S1$—$S4$ constitute the fast event trigger and provide pulse height and time of flight information for particle identification. Multiwire proportional chambers (MWPC's) were of the delay-line drift type.[16] Each of the MWPC's ($C1$—$C4$ in Fig. 2) provided both x and y information. Either pair, ($C1$ and $C3$) or ($C2$ and $C4$), is sufficient to define the focal plane trajectories, so that the other pair provides redundant information. In order to extend measurements down to very small angles, each of the chambers $C1$ and $C3$ incorporated an insensitive vertical region, created by replacing a sense wire by a thick anode wire connected to an independent power supply (shaded in Fig. 2), and $S1$—$S4$ were aligned with their vertical edges parallel to the edges of the sensitive regions. The spectrometer could then be positioned such that the beam passed, un-

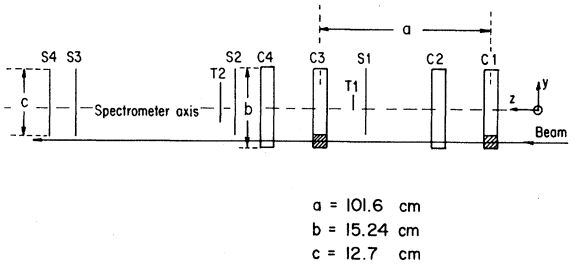

FIG. 2. Focal-plane detector assembly as seen from above. $C1$—$C4$ represent MWPC's. Each MWPC measures both x and y coordinates. The shaded regions of $C1$ and $C3$ represent insensitive regions. The trajectory of the beam is shown for a spectrometer setting of $-1.1°$. $S1$—$S4$ represent trigger scintillators. The vertical (x) dimensions of $C1$—$C4$ and $S1$—$S4$ are 15.24 cm. $T1$ and $T2$ represent smaller scintillators used to measure the electronic dead time and local chamber efficiency.

detected, as closely to the live region as permitted by the horizontal beam divergence (typically ~ 2 mrad after passing through the target) without having to pass through the massive MWPC frames. The smallest possible angles could then be reached while minimizing the background from the interaction of the beam with the detector material. Background was completely negligible. Naturally, for measurements in this mode, chambers $C2$ and $C4$ were not used.

The focal plane trajectories of scattered protons were related to those at the target by means of a transport matrix which was carefully determined by empirical means.[17] A grid of well-known trajectories was constructed by a system of wire targets and multislit collimators, and by stepping a low-intensity pencil beam over the focal plane (this procedure also permitted the absolute scattering angle to be determined accurately). This grid of trajectories was then used to determine the transport coefficients by a method of least-squares fitting.[17] As a result of this procedure, the absolute scattering angle and the solid angle could be determined within an accuracy of ± 0.5 mrad and $\pm 2\%$, respectively.

Counters $T1$ and $T2$ in Fig. 2 were small ($10.2 \times 5.1 \times 0.3$ cm) scintillation counters used to monitor the trigger efficiency and to obtain chamber efficiency locally for comparison with total chamber efficiency (they were found to agree to better than 1%).

E. Data acquisition and monitoring

For measurements at the smallest angles, the spectrometer was positioned with its axis between $-1.1°$ and $-1.2°$. In this angular range, the beam passed through the insensitive region of the detectors at the focal plane. Given the spectrometer's horizontal acceptance of 2.4°, data could be taken from $-2.4°$ (laboratory) down to a lower limit which was determined by the beam divergence and multiple Coulomb scattering in the target. Owing to multiple Coulomb scattering, the divergence of the beam increased from 0.5 mrad (FWHM) in the horizontal direction and 3.4 mrad in the vertical direction to 1.8 and 3.6 mrad, respectively (beam profiles were determined by observing the beam on the focal plane detectors). Data analysis was extended down to the smallest angle at which multiple Coulomb corrections could be made with confidence (see Sec. III A). In this configuration, only MWPC's $C1$ and $C3$ were used to detect scattered protons because MWPC's $C2$ and $C4$ were sensitive to the beam. The spectrometer was then moved outward in steps of 1° to 1.5° so as to have a region of overlap between data taken at adjacent spectrometer settings. During the first (unpolarized) stage of the experiment, differential cross sections were measured out to 4.3° (laboratory). During the second (polarized) stage, they were measured out to 4.8°, while the analyzing powers were measured out to 5.8°. (Differential cross sections between 4.8° and 5.8° were discarded due to monitor malfunction which did not, however, affect the asymmetries.)

Monitoring during the second stage was complicated by the periodic reversal of beam polarization. In both stages, a pair of "identical" threefold scintillator monitor telescopes (MT's), designed to view the target (see Fig. 1) were mounted "symmetrically" about the beam direction ($\pm 20°$ during stage 1 and $\pm 15°$ during stage 2) in the plane of scattering. Data were normalized to their combined yields (SMT). Because the geometrical symmetry about the beam direction fell short of the ideal, SMT was sensitive to the direction of the beam polarization. However, the asymmetries were small (~ 0.06) and could be corrected by standard first order techniques.[18] The effectiveness of these corrections was verified at angles $> 3.5°$, where an ion chamber could be moved into the beam without obstructing the spectrometer acceptance.

The absolute normalization of the differential cross sections was obtained during stage 1 with an accuracy of $\pm 5\%$ using a CH_2 target of known thickness as described in Ref. 4.

III. DATA REDUCTION

Data acquisition and reduction was accomplished by means of a general purpose computer program[19] which was suitably adapted to the requirements particular to this experiment. Special care was taken to calculate the kinematics and solid angle accurately. All parameters associated with the event were recorded on magnetic tape. During replay, the solid angle was defined by software cuts within an accuracy of 2%. Each data set was replayed with several different solid angle cuts and the results were found to agree within the above uncertainties. The spectrometer acceptance ($\sim 2.4°$) was divided into 20 angular bins $\sim 0.12°$ wide. The data from adjacent spectrometer settings agreed within the statistical uncertainties in the region of overlap. Since the energy resolution of the HRS was ~ 100 keV, the overall energy resolution was determined by straggling in the target material. Under these conditions, events due to scattering from heavier target constituents (e.g., ^{12}C in the windows—these events are hereafter referred to as "background") could be separated from those due to scattering from hydrogen by momentum analysis. The missing-mass spectra at 1.3° and 2.4° are shown in Fig. 3. For angles $\lesssim 2.4°$ momentum analysis had to be supplemented

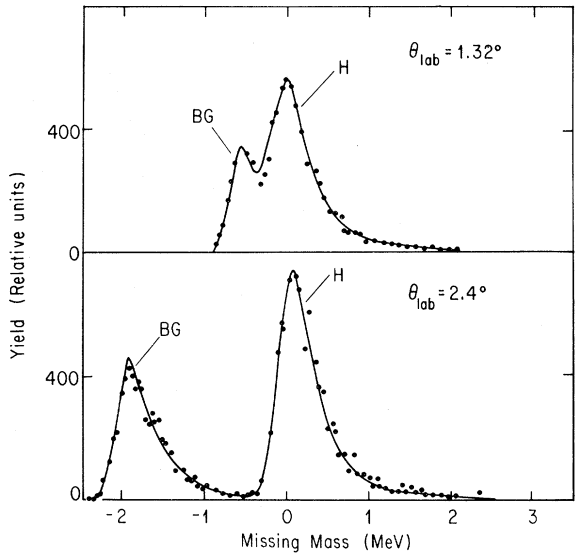

FIG. 3. Missing-mass spectra at laboratory angles of 1.32° and 2.4°. The solid curve represents the result of peak fitting. The peak labeled H corresponds to *pp* scattering. That labeled BG is due to scattering from heavier components in the target walls.

by peak-fitting techniques. The solid curves in Fig. 3 represent the results of peak fitting. Following this procedure, events due to *pp* scattering could be extracted down to 1.2° (laboratory). All the data taken with an unpolarized beam were analyzed in this manner. During the second (polarized) stage of the experiment, data were also taken with a dummy target for angles $\lesssim 2°$. These data were normalized to the background yield from the LH_2 target at $\sim 2°$, where the background peak could be clearly distinguished from that corresponding to *pp* scattering. The angular distribution of the background (for each polarization direction) could thus be determined down to very small angles (at the smallest angles, background comprised $\sim\frac{1}{3}$ of the total yield). After correcting all measurements for multiple Coulomb scattering (see Sec. III A), the background yields were subtracted from the total yields. In this way, *pp* elastic scattering data were obtained down to 0.5° (laboratory). The data below 1° are particularly valuable because they result almost entirely from Coulomb scattering. Therefore, by comparing these data with theory, the uncertainty in the absolute scattering angle could be reduced from 0.5 to 0.2 mrad. When the data obtained during the first stage of the experiment were compared with those obtained during the second, it was found necessary to shift the former to smaller angles by 0.03° (laboratory). All data were corrected for multiple Coulomb scattering as described in the next section.

A. Corrections for multiple Coulomb scattering

Multiple Coulomb scattering (MS) corrections were based on an asymptotic form of Moliere's MS theory as formulated by Bethe.[20] According to this theory, the probability that a proton scatters into an angular region $\theta,\theta+d\theta$ is given by $2\pi f(\theta)d\theta$, where,

$$f(\theta)=1/(\theta_c{}^2B)\left[\sum_0^\infty f_n(\theta)/B^n\right] \tag{3.1}$$

and θ is the laboratory polar scattering angle and (for *pp* scattering)

$$\theta_c{}^2=(0.1569)(\rho d/A)(1/p^2\beta_{\rm lab}{}^2c^2)\ , \tag{3.2}$$

$$b=B-\ln B\ ,$$
$$b=\ln[6680d/A(\beta_{\rm lab}{}^2+3.34\alpha_f{}^2)]\ , \tag{3.3}$$

where d is the target thickness (in cm), ρ is the target density (in g/cm^3), A is the atomic number, p is the c.m. momentum (in MeV/c), $\beta_{\rm lab}$ is the projectile velocity in the laboratory, and α_f is the fine-structure constant. The theory is valid for small angles ($\sin\theta\simeq\theta$) and thin targets. Recoil corrections are neglected. [The corrections for recoil effects applied in Refs. 21 and 22 are too large because the authors erroneously substituted $\beta_{\rm c.m.}$ for $\beta_{\rm lab}$ in expression (3.2).]

The zero-order term in (3.1) is a Gaussian, i.e.,

$$f_0(\theta)=2\exp(-\theta^2/w^2)\ , \tag{3.4}$$

where $w^2=\theta_c{}^2B$. $f_0(\theta)$ determines the shape of $f(\theta)$ at very small angles ($\theta/w\lesssim 2$). The higher-order terms become significant at larger angles, causing $f(\theta)$ to decrease more slowly with increasing θ. At these angles, one can apply an asymptotic expression devised by Bethe,[20] viz.,

$$R^{-1}=1-4(\theta/w)^{-2}[1+2B^{-1}\ln(0.4\theta/w)]\ , \tag{3.5}$$

where $R=f(\theta)/f_R(\theta)$, f_R being the Rutherford single-scattering distribution in the laboratory. Bethe showed that this approximation is excellent down to $\theta/w\simeq 2.4$, i.e., down to the point where the Gaussian term begins to dominate. In the case of this work, θ/w was ~ 6 at the smallest angle (0.5°). The asymptotic expression (3.5) could therefore be applied, but it needed to be modified at the smallest angles to account for the effects of finite beam divergence. Cormack[23] showed how these effects could be accounted for when the beam divergence has no azimuthal dependence. In the case of this work, however, the beam divergence *did* have an azimuthal dependence. The effects of arbitrary beam

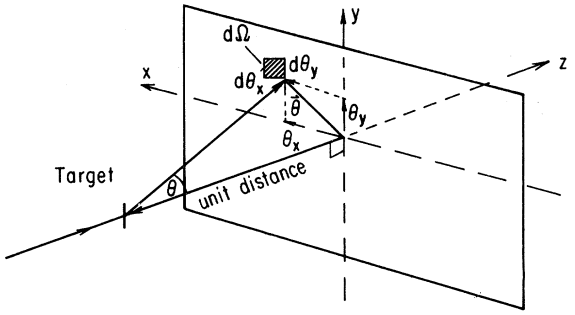

FIG. 4. The small-angle approximation. The polar scattering angle is represented by a vector $\vec{\theta}$ in a plane (x,y) which is normal to the beam direction (z) and unit distance from the target. The solid angle $d\Omega$ is given by an element of area $d\theta_x d\theta_y$ (shaded).

divergence may be estimated by Monte Carlo methods.[24] However, when the beam divergence has an ellipsoidal envelope, as was the case for this work, one can, as shown below, treat them analytically to a good approximation.

The small-angle approximation is implicit in the Moliere theory. In this approximation, the polar angle may be represented by a vector in a plane normal to the direction of the projectile and unit distance from the target (the dimensions of the target along the beam direction are assumed to be negligible), as shown in Fig. 4. Its projections along the vertical and horizontal axes define angles θ_x and θ_y. An element of solid angle $d\Omega$ corresponds to an element of area, i.e., $d\Omega = d\theta_x d\theta_y$. A beam divergence having an ellipsoidal envelope may be described by

$$b(\theta_x,\theta_y)d\Omega = (1/\pi w_x w_y)\exp(-\theta_x^2/w_x^2) \times \exp(-\theta_y^2/w_y^2)d\theta_x d\theta_y \ . \quad (3.6)$$

Vertical (w_x) and horizontal (w_y) widths were found to be 2.06 and 0.30 mrad, respectively. The modified MS distribution function f_M can then be expressed as a two-dimensional convolution of $b(\theta_x,\theta_y)$ and $f(\theta)$, i.e.,

$$f_M(\theta)=(1/\pi w_x w_y)\int\int f(|\vec{\theta}-\vec{\theta}'|)\exp(-\theta_x'^2/w_x^2)\exp(-\theta_y'^2/w_y^2)d\theta_x' d\theta_y' \ . \quad (3.7)$$

Now, $f(\theta)$ can be written in terms of (3.5), i.e.,

$$f(\theta)\simeq R f_R(\theta) \ , \quad (3.8)$$

where

$$f_R(\theta)=2\theta_c^2/\theta^4 \ ,$$

and, since R varies little over $\Delta\theta\simeq(w_x^2+w_y^2)^{1/2}$, it can be taken outside the integral, i.e.,

$$f_M(\theta)\simeq(R/\pi w_x w_y)\int\int f_R(|\vec{\theta}-\vec{\theta}'|)\exp(-\theta_x'^2/w_x^2)\exp(-\theta_y'^2/w_y^2)d\theta_x' d\theta_y' \ . \quad (3.9)$$

Now, by writing

$$f_R(|\vec{\theta}-\vec{\theta}'|)=2(\theta_c^2/\theta^4)(\theta^4/|\vec{\theta}-\vec{\theta}'|^4) \ , \quad (3.10)$$

and noting that $\theta \gg w_x$ and $\theta \gg w_y$, $f_R(|\vec{\theta}-\vec{\theta}'|)$ may be written as a binomial expansion and (3.9) can be integrated term-by-term to obtain

$$f_M(\theta)=R(\theta)f_R(\theta)[1-(w_x/\theta)^2-(w_y/\theta)^2+6\cos^2\phi(w_x^2/\theta)+6\sin^2\phi(w_y/\theta)^2+\cdots] \ , \quad (3.11)$$

where ϕ is the azimuthal angle in the laboratory. It was found sufficient to retain only those terms shown in (3.11). Since w_y is small ($w_y=0.3$ mrad), only the data at the smallest angles ($\theta \lesssim 1°$), where the azimuthal angle is significant ($\Delta\phi\simeq 60°$), were significantly affected by the beam divergence. MS corrections at the smallest angle (0.5°) were 6% and less than 1% beyond 1.4°.

IV. RESULTS

The differential elastic cross sections $\sigma(\theta)$ determined with an unpolarized beam are given in Table I. They have already been published in graphical form[4] but have since been shifted to smaller angles by 0.03° for reasons outlined in Sec. III. Differential cross sections and analyzing powers $A(\theta)$ obtained during the second (polarized) stage of the experiment are given in Tables II and III and plotted in Figs. 5 and 6. The uncertainties are purely statistical. Absolute uncertainties are ±5% for both $\sigma(\theta)$ and $A(\theta)$. These data extend to considerably smaller angles than those of other experiments. Other measurements reported[11,25,26] at this energy are also plotted in Figs. 5 and 6 (for reasons of clarity not all data from Ref. 11 were plotted in Figs. 5 and 6). Both $\sigma(\theta)$ and $A(\theta)$ agree very well with those of Ref. 11. One should note that these authors claim

TABLE I. *pp* differential elastic cross sections obtained with 800 MeV unpolarized protons. Uncertainties ($\pm\Delta\sigma$) are purely statistical. Absolute uncertainties are ±5%.

θ_{lab} deg	$\theta_{c.m.}$ deg	$\sigma(\theta_{c.m.})$ mb/sr	$\Delta\sigma$ mb/sr
1.21	2.90	67.2	2.7
1.33	3.18	47.9	2.2
1.40	3.35	41.4	1.1
1.44	3.45	39.3	1.9
1.52	3.63	33.8	1.0
1.56	3.72	33.1	1.7
1.63	3.90	30.5	0.7
1.67	4.00	27.9	1.5
1.75	4.17	25.6	0.5
1.79	4.27	24.6	1.4
1.86	4.45	23.7	0.5
1.90	4.54	23.5	1.3
1.98	4.72	22.2	0.4
2.02	4.82	21.7	1.2
2.09	4.99	20.7	0.4
2.21	5.27	19.6	0.4
2.32	5.54	19.3	0.4
2.43	5.81	18.9	0.4
2.50	5.97	18.2	0.4
2.55	6.09	17.5	0.4
2.61	6.24	17.1	0.4
2.66	6.36	17.3	0.4
2.73	6.52	16.9	0.4
2.78	6.63	16.9	0.4
2.84	6.79	16.9	0.4
2.89	6.91	16.2	0.4
2.96	7.06	16.6	0.4
3.01	7.18	16.3	0.4
3.07	7.34	16.1	0.4
3.12	7.46	16.0	0.4
3.19	7.61	16.2	0.4
3.24	7.73	16.0	0.6
3.30	7.88	15.4	0.4
3.39	8.08	15.6	0.3
3.42	8.16	15.5	0.4
3.50	8.36	15.1	0.3
3.53	8.43	14.8	0.5
3.61	8.63	15.0	0.3
3.65	8.70	14.8	0.5
3.73	8.90	14.7	0.3
3.84	9.18	14.6	0.3
3.96	9.45	15.0	0.3
4.07	9.72	15.0	0.3
4.19	9.99	14.9	0.5
4.30	10.27	14.7	0.5

an absolute uncertainty of ±3% for $\sigma(\theta)$. The excellent agreement between these two sets of data implies that the Gatchina cross sections[25] (see Fig. 5) are too small by 11%. Our analyzing powers also agree very well with those of Ref. 26.

TABLE II. *pp* differential elastic cross sections obtained with 800 MeV polarized protons. Uncertainties ($\pm\Delta\sigma$) are purely statistical. These data are normalized to those given in Table I.

θ_{lab} deg	$\theta_{c.m.}$ deg	$\sigma(\theta_{c.m.})$ mb/sr	$\Delta\sigma$ mb/sr
0.50	1.19	1813	91
0.64	1.53	671	33
0.78	1.87	318	16
0.93	2.21	166.6	8.4
1.07	2.55	102.1	3.0
1.21	2.87	65.2	1.9
1.36	3.24	48.0	1.4
1.43	3.42	37.5	1.4
1.50	3.58	37.0	1.2
1.57	3.76	31.5	0.9
1.64	3.92	27.0	1.2
1.72	4.10	27.5	1.8
1.79	4.27	27.0	1.4
1.86	4.44	24.2	0.7
1.93	4.61	22.2	1.1
2.00	4.71	21.9	0.9
2.07	4.95	20.8	1.0
2.15	5.12	20.0	0.5
2.29	5.46	19.6	0.5
2.43	5.81	18.4	0.6
2.57	6.15	18.0	0.3
2.72	6.49	17.4	0.3
2.86	6.83	16.5	0.3
3.00	7.17	16.3	0.4
3.14	7.50	16.2	0.4
3.29	7.85	15.6	0.4
3.36	8.02	15.3	0.4
3.43	8.20	15.6	0.4
3.50	8.36	15.7	0.5
3.58	8.54	15.6	0.4
3.64	8.70	15.2	0.5
3.79	9.04	15.3	0.5
3.93	9.38	15.7	0.5
4.07	9.73	15.2	0.5
4.22	10.07	15.6	0.5
4.36	10.41	15.5	0.5
4.50	10.75	16.1	0.5
4.57	10.92	15.0	0.8
4.65	11.09	15.4	0.5
4.71	11.25	16.0	0.9
4.79	11.43	14.5	0.5

Also plotted in Figs. 5 and 6 are the predictions of phase-shift analyses by Bystricky *et al.*,[27] Arndt *et al.*,[28] and Hoshizaki *et al.*[3,29] The first two analyses include preliminary values of our data. Since these differ little from the data tabulated in Tables I–III, inclusion of these final data should make little difference. The solid lines in Figs. 5 and 6

TABLE III. Analyzing powers for *pp* elastic scattering at 800 MeV. Uncertainties ($\pm\Delta A$) are purely statistical. Absolute uncertainties are ±5%.

θ_{lab} deg	$\theta_{c.m.}$ deg	A	ΔA
0.50	1.19	0.001	0.015
0.71	1.70	0.022	0.014
0.86	2.04	0.020	0.012
1.07	2.55	0.038	0.008
1.21	2.88	0.034	0.010
1.43	3.42	0.071	0.008
1.57	3.76	0.067	0.009
1.64	4.04	0.073	0.012
1.87	4.45	0.103	0.008
1.97	4.69	0.103	0.012
2.00	4.78	0.106	0.010
2.15	5.12	0.117	0.009
2.29	5.46	0.124	0.009
2.48	5.91	0.142	0.009
2.64	6.30	0.151	0.009
2.78	6.64	0.150	0.012
2.84	6.79	0.173	0.012
3.10	7.40	0.178	0.010
3.26	7.79	0.187	0.010
3.37	8.05	0.189	0.015
3.64	8.69	0.195	0.012
3.79	9.04	0.206	0.011
3.93	9.38	0.206	0.011
4.07	9.73	0.217	0.011
4.29	10.24	0.222	0.010
4.53	10.81	0.239	0.010
4.71	11.25	0.236	0.007
4.86	11.60	0.260	0.009
4.98	11.90	0.245	0.009
5.13	12.25	0.269	0.009
5.29	12.62	0.275	0.008
5.43	12.96	0.274	0.010
5.57	13.30	0.295	0.010
5.72	13.64	0.295	0.012
5.86	13.98	0.304	0.012

represent the results of an analysis to be described in the next section.

V. ANALYSIS

The data were analyzed, as described below, in order to extract information about the zero-degree amplitudes. The *pp* scattering matrix was parametrized as in (1.1). Each of the component amplitudes may be separated into nuclear (subscript N) and electromagnetic terms (subscript E), i.e.,

$$X(t)=X_N(t)+X_E(t)\ ,$$
$$X(t)=X_N(t)+X'_E(t)\exp(i\Delta)\ , \tag{5.1}$$

where $X=\alpha$, β, γ, δ, or ϵ. X_N is the "contaminated"[30] nuclear amplitude. It is this amplitude which is extracted from the analysis. X_N may be expressed as $X_N^P+0(\alpha_f)$ (α_f is the fine-structure constant) where $0(\alpha_f)$ arises from higher-order electromagnetic corrections to the "pure" nuclear amplitude X_N^P. (In fact, X_N^P is not altogether free of em contamination.[30] However, this additional contamination is impossible to calculate and we make the customary assumption that it is negligible.) Model-dependent prescriptions for calculating $0(\alpha_f)$ have been given by Buttimore *et al.*[30] The magnitude of their effects on the results of the analysis have been found to be negligible. $X'_E(t)$ may be written $X''_E(t)F^2$, where $X''_E(t)$ is the one-photon exchange amplitude and F^2 is the proton form factor, given by[32]

$$F=1/(1+|t|/0.71)^2$$

(magnetic form factors have been neglected since they are negligibly small). $\Delta(t)$ is known as the "relative phase" and accounts for higher-order em corrections. In the general case, it may be written

$$\Delta(t)=-\alpha_f\ln(r|t|)+k\ , \tag{5.2}$$

where r and k are model-dependent constants[31] which may be different for different amplitudes. Since variation of these parameters is equivalent to varying the $0(\alpha_f)$ corrections to the nuclear amplitudes, one would expect their effect on the analysis to be weak. This has been shown to be the case.[31] We have arbitrarily used the expression given by Bethe,[33] i.e.,

$$\Delta(t)=(2\alpha_f/\beta_{lab})\ln(0.209/\sqrt{|t|})\ , \tag{5.3}$$

for all amplitudes, where β_{lab} is the velocity of the incident proton in the laboratory frame and t is in units of $(\mathrm{GeV}/c)^2$. Of the one-photon-exchange amplitudes, $\alpha''_E(\sim 1/t)$ and $\gamma''_E(\sim 1/\sqrt{|t|})$ are found to be significant at small angles, whereas the others are insignificantly small everywhere. Therefore, one may set $\beta_E=\epsilon_E=\delta_E=0$ and write

$$\sigma(\theta)=|\alpha_N+\alpha_E|^2+|\gamma_N+\gamma_E|^2+S\ , \tag{5.4}$$

where

$$S=|\beta_N|^2+|\delta_N|^2+|\epsilon_N|^2\ .$$

It is convenient to distinguish between nuclear, em, and interference terms, i.e.,

$$\sigma=\sigma_N+\sigma_I+\sigma_E\ ,$$

where

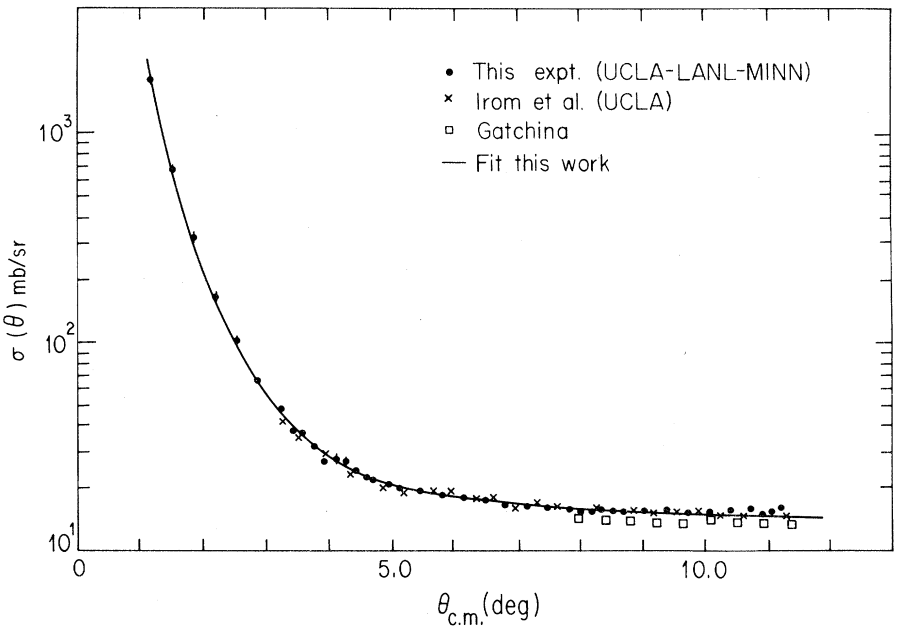

FIG. 5. Differential cross sections for *pp* elastic scattering at 800 MeV. Only the results obtained with a polarized beam are shown. Also plotted are some of the data from Refs. 11 and 25. The solid line represents the result of the analysis described in Sec. V. Predictions of current phase-shift analyses (Refs. 3 and 27–29) are indistinguishable from this line.

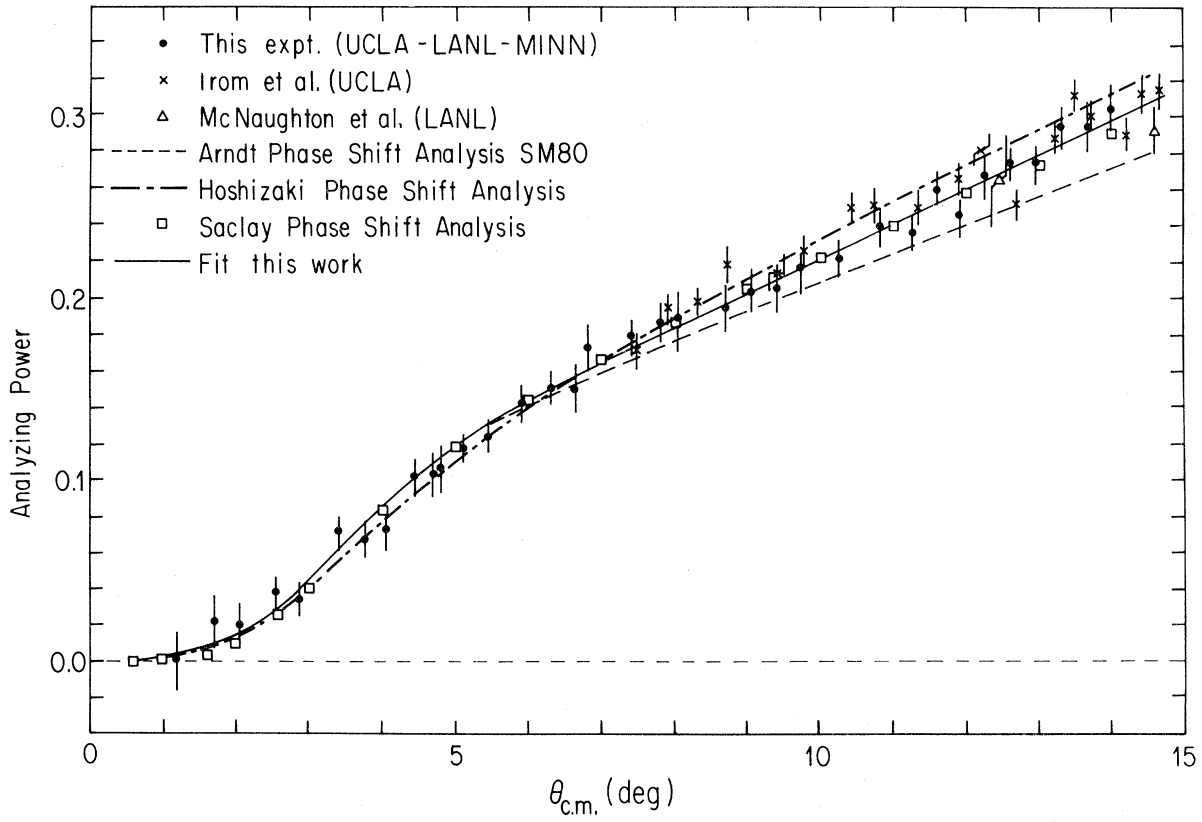

FIG. 6. Analyzing powers (A) for *pp* elastic scattering at 800 MeV. Also plotted are the results of other measurements (Refs. 11 and 26) at this energy. The predictions of current phase-shift analyses (Refs. 3 and 27–29) and of an analysis performed in this work (see Sec. V) are also shown.

$$\sigma_N = |\alpha_N|^2 + |\gamma_N|^2 + S ,$$
$$\sigma_I = 2\,\mathrm{Re}(\alpha_N^* \alpha_E) + 2\,\mathrm{Re}(\gamma_N^* \gamma_E) , \quad (5.5)$$
$$\sigma_E = |\alpha_E|^2 + |\gamma_E|^2 .$$

The t dependence of $\alpha_N(t)$ is parametrized in terms of the conventional slope parameter b, i.e.,

$$|\alpha_N(t)|^2 = |\alpha_N(0)|^2 \exp(b_1 t) , \quad (5.6)$$

and a similar t dependence is assumed for $S(t)$, viz.,

$$S(t) = S(0)\exp(b_2 t) . \quad (5.7)$$

b_1 may be estimated from the slope of $\sigma(t)$ at higher momentum transfer.[34] b_2 is not so easy to estimate but theoretical arguments may be made[35] suggesting that its magnitude should be comparable to that of b_1. Fortunately, because of the small t range spanned by the data, the analysis is relatively insensitive to the values of b_1 and b_2, within a range of reasonable values. For small θ the θ dependence of γ_N at small angles is given, to a good approximation, by[1]

$$i\gamma_N(\theta) = h_N(0)\sin(\theta) . \quad (5.8)$$

Then, using the definition of ρ (see Sec. I) and the optical theorem [e.g., (1.3)] one can write,

$$\sigma_N = (p\sigma_{\mathrm{tot}}/4\pi\hbar)^2(1+\rho^2)[\exp(b_1 t) + R\exp(b_2 t)] + |h_N(0)|^2 \sin^2\theta ,$$
$$\sigma_I = (2p\sigma_{\mathrm{tot}}/4\pi\hbar)(\rho\cos\Delta + \sin\Delta)\exp(b_1 t/2)\alpha_E' + 2[\mathrm{Im}h_N(0)\cos\Delta - \mathrm{Re}h_N(0)\sin\Delta]\gamma_E'\sin\theta , \quad (5.9)$$
$$\sigma_E = |\alpha_E'|^2 + |\gamma_E'|^2 ,$$

where $R = S(0)/|\alpha_N(0)|^2$.

For the analyzing powers, one may write

$$\sigma A = 2\,\mathrm{Re}[(\alpha+\beta)^*(i\gamma)] . \quad (5.10)$$

Once again, it is convenient to distinguish between nuclear, interference, and em terms, i.e.,

$$(\sigma A)_N = 2[(\mathrm{Im}\alpha_N + \mathrm{Im}\beta_N)\mathrm{Re}\gamma_N - (\mathrm{Re}\alpha_N + \mathrm{Re}\beta_N)\mathrm{Im}\gamma_N] ,$$

$$(\sigma A)_I = 2[\mathrm{Re}\gamma_E(\mathrm{Im}\alpha_N + \mathrm{Im}\beta_N) + \mathrm{Im}\alpha_E\mathrm{Re}\gamma_N - \mathrm{Im}\gamma_E(\mathrm{Re}\alpha_N + \mathrm{Re}\beta_N) - \mathrm{Re}\alpha_E\mathrm{Im}\gamma_N] , \quad (5.11)$$

$$(\sigma A)_E = 2[\mathrm{Im}\alpha_E\mathrm{Re}\gamma_E - \mathrm{Re}\alpha_E\mathrm{Im}\gamma_E] .$$

From our previous determination[4] of the value of R, one would suspect that terms including the amplitudes β_N are small. The predictions of a current phase shift analysis[28] confirm this suspicion. The predictions for all terms including the amplitude β_N are plotted in Fig. 7 together with the dominant terms for comparison. It is clear from this figure that the terms including β_N are much smaller than the dominant ones. Their omission is not expected to influence the analysis significantly while reducing the number of unknowns. Since the remaining interference terms which include higher-order em amplitudes (i.e., $\mathrm{Im}\gamma_E$ and $\mathrm{Im}\alpha_E$) are of comparable magnitude, they are also excluded. The pure em term is completely negligible at these angles. With these approximations, one then obtains

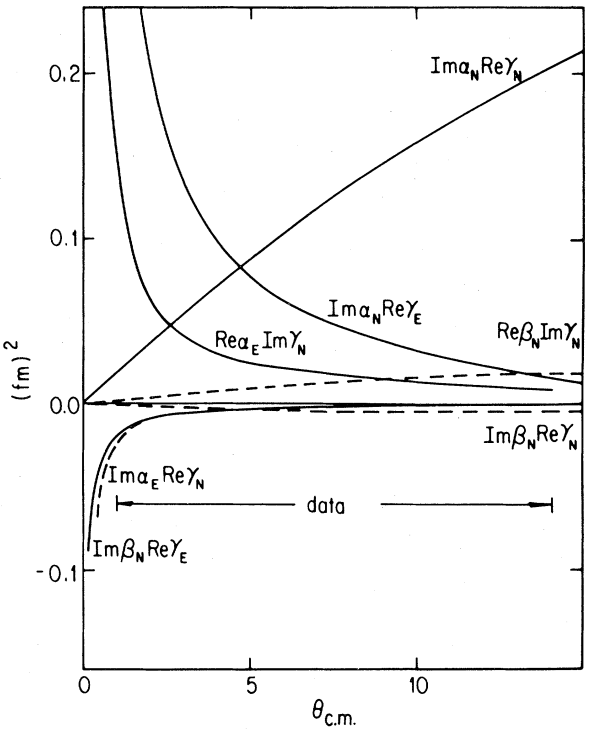

FIG. 7. Some of the terms contributing to the pp analyzing powers at 800 MeV. The upper limits for the remaining terms are as follows:

$$|\mathrm{Re}\alpha_N\mathrm{Im}\gamma_N| < 5\times10^{-4} ,$$
$$|\mathrm{Re}\alpha_N\mathrm{Im}\gamma_E| < 10^{-3} ,$$
$$|\mathrm{Re}\beta_N\mathrm{Im}\gamma_E| < 5\times10^{-3} ,$$

for $1° < \theta_{\mathrm{c.m.}} < 15°$. pp amplitudes were taken from the phase-shift analysis SM80 of Arndt *et al.* (Ref. 28).

TABLE IV. Parameters extracted from the analysis performed in this work. See text for definitions. $(\chi')^2$ refers to the χ^2 per degree of freedom. Uncertainties are purely statistical. An asterisk indicates that the parameter was kept fixed.

OF deg	N	b_1 $(\text{GeV}/c)^{-2}$	b_2 $(\text{GeV}/c)^{-2}$	ρ	R	$\text{Im}h_N(0)$ fm	$\text{Re}h_N(0)$ fm	$(\chi')^2$
0.0*	1.0*	8.0*	2.0*	−0.046 ±0.013	0.145 ±0.006	0.74 ±0.01	−0.02 ±0.05	1.13
0.0*	1.0*	10.0*	8.0*	−0.031 ±0.013	0.172 ±0.007	0.75 ±0.02	−0.02 ±0.05	1.15
0.0*	1.0*	8.0*	8.0*	−0.043 ±0.014	0.155 ±0.007	0.74 ±0.02	−0.03 ±0.04	1.17
0.0*	1.0*	8.0*	15.0*	−0.040 ±0.007	0.163 ±0.014	0.73 ±0.03	−0.05 ±0.04	1.21
0.02*	1.0*	8.0*	15.0*	−0.018 ±0.008	0.177 ±0.016	0.74 ±0.01	−0.02 ±0.04	1.35
0.0*	0.98*	8.0*	8.0*	−0.026 ±0.012	0.140 ±0.010	0.74 ±0.02	−0.02 ±0.04	1.22

$$(\sigma A)_N \simeq 2[\text{Im}\alpha_N \text{Re}\gamma_N - \text{Im}\gamma_N \text{Re}\alpha_N] ,$$
$$(\sigma A)_I \simeq 2[\text{Im}\alpha_N \text{Re}\gamma_E - \text{Im}\gamma_N \text{Re}\alpha_E] . \quad (5.12)$$

Then, assuming t dependences as defined by Eqs. (5.6)–(5.8) and using the definition of ρ (see Sec. I) and the optical theorem [Eq. (1.3)] one obtains

$$(\sigma A)_N = (2p\sigma_{\text{tot}}/4\pi\hbar)\exp(b_1 t/2) \times[\rho \text{Re}h_N(0) + \text{Im}h_N(0)]\sin\theta ,$$
$$(\sigma A)_I = [(2p\sigma_{\text{tot}}/4\pi\hbar)\exp(b_1 t/2)\gamma'_E + \text{Re}h_N(0)\alpha'_E \sin\theta]\cos\Delta . \quad (5.13)$$

For the one-photon-exchange amplitudes[36] α''_E and γ''_E, only the divergent terms are retained, i.e.,

$$\alpha''_E \simeq \alpha_f \alpha_0 / t ,$$

where

$$\alpha_0 = 2\hbar p/\beta_{\text{lab}} = \hbar(s - 2m^2)/\sqrt{s}$$

and (5.14)

$$\gamma''_E = \alpha_f \gamma_0 / \sqrt{|t|} ,$$

where

$$\gamma_0 = (1/\sqrt{s})[(\sqrt{s} - 2m)/(\sqrt{s} + 2m)]^{1/2} \times F^2[(\sqrt{s} + m) + (1/2m)(\mu - 1)\sqrt{s}(\sqrt{s} + 2m)] ,$$

s is the invariant mass ($s = 2mE_{\text{lab}} + 2m^2$), m is the proton mass, and $c = 1$.

Differential cross sections and analyzing powers were parametrized according to Eqs. (5.9) and (5.13), respectively, and fitted to the data by the method of least-squares fitting. ρ, R, $\text{Re}h_N(0)$, and $\text{Im}h_N(0)$ were allowed to vary simultaneously in order to ob-

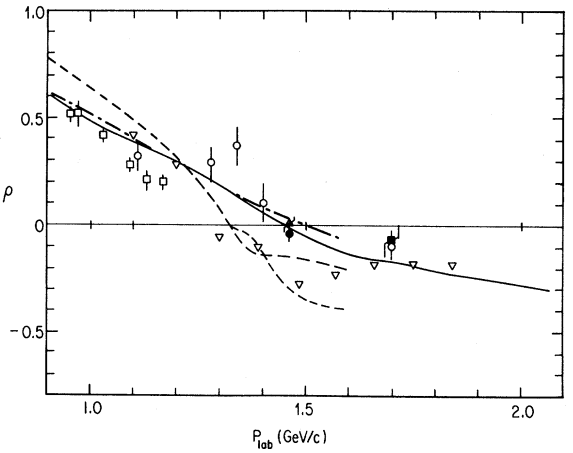

FIG. 8. Ratio ρ of the real to imaginary parts of the spin-independent amplitude plotted as a function of laboratory momentum. Data: □, Aebischer *et al.* (Ref. 37); ○, Vorobyov *et al.* (Ref. 8); ■, Dowell *et al.* (Ref. 39); ▲, Irom *et al.* (Ref. 11); ●, this experiment. Phase-shift analyses: – – –, Bystricky *et al.* (Ref. 27); —·—·—, Arndt *et al.* (Ref. 28); ▽, Hoshizaki *et al.* (Refs. 3 and 29). The solid line represents the FDR calculations of Grein and Kroll (Ref. 2).

tain best fits to both $\sigma(\theta)$ and $A(\theta)$. The analysis was performed for various values of the slope parameters b_1 and b_2. A sample of the results (see Table IV) shows that the results of the analysis depend only weakly on these parameters. However, they depend relatively strongly on the absolute angular offset (OF) and, to a lesser extent, on the absolute normalization (N). The uncertainties quoted in Table IV are purely statistical (i.e., from the error matrix). In order to estimate the overall uncertainties, all contributions were assumed to add incoherently so that the following prescription was adopted:

$$(\Delta x)^2=(\Delta x_{\rm OF})^2+(\Delta x_N)^2+(\Delta x_{b_1})^2 +(\Delta x_{b_2})^2+(\Delta x_{\rm stat})^2 , \quad (5.15)$$

where $x=\rho$, R, $\mathrm{Re}h_N(0)$, or $\mathrm{Im}h_N(0)$. $x_{\rm OF}$ is the uncertainty in x corresponding to an uncertainty of 0.02° (laboratory) in the absolute angle, and x_N is that due to the uncertainty in the absolute normalization. Given the excellent agreement between these data and those of Ref. 11, we estimate N to be $\pm 2\%$ for $\sigma(\theta)$. For the analyzing powers, an absolute uncertainty of $\pm 5\%$ is assumed to arise from a corresponding one in the beam polarization. Δx_{b_1} and Δx_{b_2} are the uncertainties in the slope parameters and were taken to be ± 4 $(\mathrm{GeV}/c)^{-2}$ and ± 6 $(\mathrm{GeV}/c)^{-2}$, respectively. An additional uncertainty of ± 0.05 fm is added in quadrature to that calculated for $\mathrm{Re}h_N(0)$ according to Eq. (5.15), in order to account for the omission of terms including β_N from the analysis. For the most probable values of b_1 and b_2, i.e., for $b_1=8$ $(\mathrm{GeV}/c)^{-2}$ and $b_2=8$ $(\mathrm{GeV}/c)^{-2}$, the following values were obtained:

$$\rho=-0.04\pm 0.04 ,$$

$$R=0.16\pm 0.03 ,$$

$$\mathrm{Im}h_N(0)=+0.74\pm 0.04 \text{ fm} ,$$

$$\mathrm{Re}h_N(0)=-0.03\pm 0.08 \text{ fm} .$$

The solid curves shown in Figs. 5 and 6 correspond to these values.

VI. DISCUSSION

Results from the analysis of these data are plotted as a function of (laboratory) projectile momentum in Figs. 8–11, together with those from other experiments[8,11,37,38] between 1 and 2 GeV/c (the data from Refs. 6, 7, and 39 were excluded since they disagree with all the other data). Only the data of Ref. 11 are of an accuracy comparable to these. The results of their analysis for ρ, R, and $\mathrm{Im}h_N(0)$ are in remarkably good agreement with ours, whereas that for $\mathrm{Re}h_N(0)$ is not. This is not surprising because their measurements of $A(\theta)$ did not extend to angles smaller than 7° (c.m.). As is clear from Fig. 7, $\mathrm{Im}h_N(0)$ is determined by the term

$$\mathrm{Im}\alpha_N \mathrm{Re}\gamma_N \ (\simeq \mathrm{Im}\alpha_N \mathrm{Im}h_N(0)\sin\theta) .$$

This term is enhanced by the large value of $\mathrm{Im}\alpha_N$ at intermediate energies and it clearly determines the angular dependence of $A(\theta)$ for angles $\gtrsim 5°$ (c.m.). It is therefore sufficient to measure $A(\theta)$ at angles greater than this in order to extract $\mathrm{Im}h_N(0)$. On

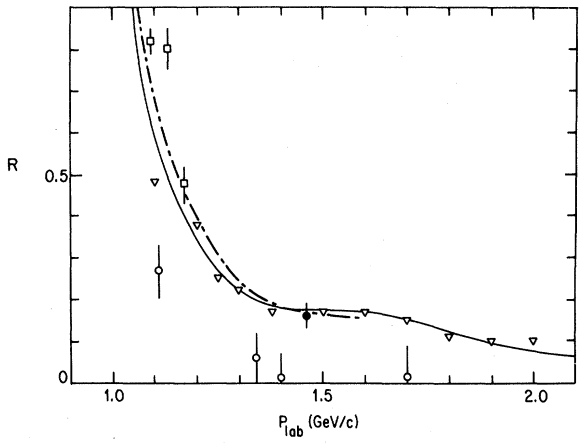

FIG. 9. R plotted as a function of laboratory momentum. Data: □, Aebischer *et al.* (Ref. 37); ○, Vorobyov *et al.* (Ref. 8); ●, this experiment. The data of Irom *et al.* (Ref. 11) are indistinguishable from ours. Phase-shift analyses: —·—·—, Arndt *et al.* (Ref. 28); ∇, Hoshizaki *et al.* (Ref. 29). The solid line represents the result of the FDR calculations of Grein and Kroll (Ref. 2).

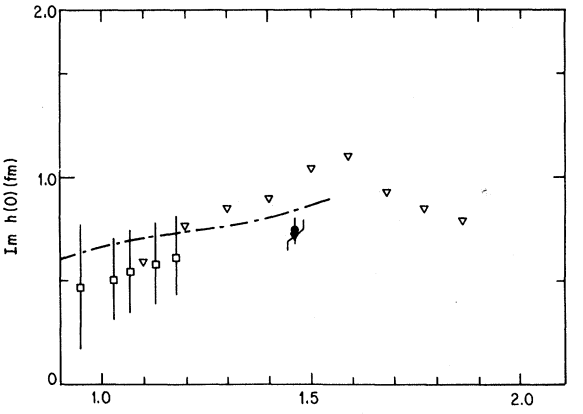

FIG. 10. $\mathrm{Im}h_N(0)$ plotted as a function of laboratory momentum. Data: □, Aebischer *et al.* (Ref. 10); ▼, Irom *et al.* (Ref. 11); ●, this experiment. Phase-shift analyses are the same as in Fig. 9.

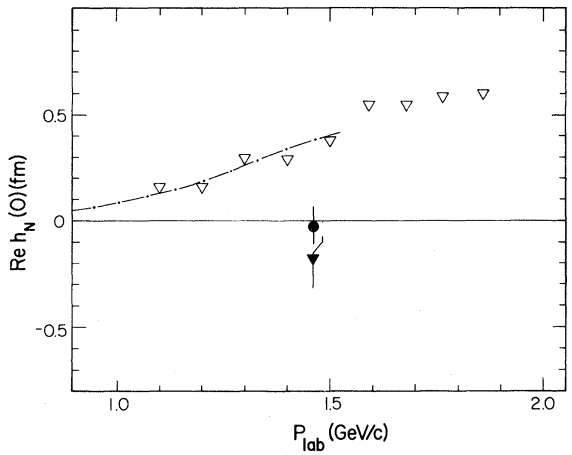

FIG. 11. Re$h_N(0)$ as a function of laboratory momentum. Data: ▼, Irom *et al.* (Ref. 11); ●, this experiment. Phase-shift analyses: —·—·—, Arndt *et al.* (Ref. 28); ∇, Hoshizaki *et al.* (Ref. 29).

the other hand, Re$h_N(0)$ is determined by the term

$$\mathrm{Re}\alpha_E \mathrm{Im}\gamma_N \ (\simeq \mathrm{Re}\alpha_E \mathrm{Re}h_N(0)\sin\theta)$$

which is enhanced by the $(1/t)$ singularity of α_E. It therefore becomes significant at smaller angles. It is clear from Fig. 7 that it is necessary to measure $A(\theta)$ at angles $\lesssim 3°$ (c.m.) in order to extract Re$h_N(0)$. Even so, the contribution to $A(\theta)$ of $\mathrm{Im}\alpha_N \mathrm{Re}\gamma_E$ in this angular range is considerably greater (see Fig. 7), but this contribution is very well determined since its uncertainty depends only on that of Imα_N, which is very small. Nevertheless, statistical uncertainties from the analysis of Re$h_N(0)$ are comparatively large (see Table IV). Another factor contributing to the uncertainty in Re$h_N(0)$ is the omission of terms depending on the double-spin-flip amplitudes (see Sec. V). However, it can be seen from Fig. 7 that these terms are relatively unimportant for $\theta \gtrsim 1°$.

The predictions of some current phase-shift analyses,[3,27–29] and of FDR calculations[2] (for ρ and R) are also shown for comparison in Figs. 8—11. Agreement between these predictions and the results of our analyses is good for ρ and R, reasonable for Im$h_N(0)$, and poor for Re$h_N(0)$. The reason for this latter discrepancy is unknown.

The good agreement between experiment, phase shift analyses, and FDR calculations in the case of R is of particular significance. This value of R implies that

$$2\,|\,\mathrm{Re}\beta_N(0)\,|^2 + |\,\mathrm{Re}\epsilon_N(0)\,|^2$$

is comparatively large, which in turn implies that structure comparable to that seen in the imaginary components of the double spin-flip amplitudes[2,40] also exists in their real components. Such structure is relevant to speculations[2,40,41] concerning the existence of dibaryon resonances. One should note that uncertainties in the empirical value of R have been considerably reduced by inclusion of $A(\theta)$ in our analysis.

VII. CONCLUSION

Differential elastic cross sections and analyzing powers for *pp* elastic scattering have been measured at 800 MeV for laboratory angles ranging between 0.5° and 4.8°, in the case of the former, and 0.5° and 5.9°, in the case of the latter. Measurements below 1°, where the cross section is virtually pure Coulomb, have permitted the absolute angle to be determined to ±0.02°. After correction for multiple Coulomb scattering effects, these data were analyzed in terms of the *pp* scattering amplitudes which were assumed to have a Gaussian t dependence. Empirical values for parameters related to their zero-degree values, viz., ρ, R, Re$h_N(0)$, and Im$h_N(0)$ (see text for definitions), were extracted from the analysis. Analyzing power data below 1.5° in the laboratory were found indispensable to the determination of Re$h_N(0)$. The results of our analysis were compared with the results of other experiments and with the predictions of current phase shift analyses. Agreement was good except in the case of Re$h_N(0)$.

ACKNOWLEDGMENTS

We wish to thank the cryogenics group at LAMPF for constructing the LH target, C. L. Morris for constructing the MWPC's, and G. W. Hoffmann and Bo Hoistad for beam tuning. We also wish to thank F. Irom for communicating his data to us prior to publication. This work was supported in part by the U. S. Department of Energy.

*Present address: Department of Physics, University of South Carolina, Columbia, SC 29208.
†Present address: Los Alamos National Laboratory, Los Alamos, NM 87545.
‡Present address: Department of Physics, Jordan University, Amman, Jordan.

[1] L. Wolfenstein, Annu. Rev. Nucl. Sci. 6, 43 (1956); N. Hoshizaki, Prog. Theor. Phys. Suppl. 42, 107 (1968); J. Bystricky, F. Lehar, and P. Winternitz, J. Phys. (Paris) 1, 1 (1978).
[2] W. Grein and P. Kroll, Nucl. Phys. B137, 173 (1978).
[3] N. Hoshizaki, Prog. Theor. Phys. 60, 1796 (1978).

[4]A. Wriekat *et al.*, Phys. Lett. 97B, 33 (1980).
[5]L. Ray *et al.*, Phys. Rev. C 23, 828 (1981).
[6]L. M. C. Dutton, R. Howells, J. Jafar, and H. Van der Raay, Phys. Lett. 25B, 245 (1967).
[7]L. M. C. Dutton *et al.*, Phys. Lett. 26B, 679 (1968).
[8]A. A. Vorobyov *et al.*, Phys. Lett. 41B, 639 (1972).
[9]D. Besset *et al.*, Phys. Rev. D 21, 580 (1980).
[10]D. Aebischer *et al.*, Nucl. Phys. A276, 445 (1977).
[11]F. Irom, G. J. Igo, J. B. McClelland, and C. A. Whitten, Jr., Phys. Rev. C 25, 373 (1982).
[12]B. Zeidman, Los Alamos Scientific Laboratory Report LA-4773-MS, 1971 (unpublished).
[13]M. W. McNaughton, Los Alamos Scientific Laboratory Report LA-8307-MS, 1980 (unpublished).
[14]G. G. Ohlsen, Los Alamos Scientific Laboratory Report LA-4451, 1970 (unpublished).
[15]M. W. McNaughton *et al.*, Phys. Rev. C 23, 1128 (1981).
[16]C. L. Morris, H. A. Thiessen, and G. W. Hoffman, IEEE Trans. Nucl. Sci., NS-25, 141 (1978).
[17]R. L. Boudrie *et al.*, IEEE Trans. Nucl. Sci. NS-26, 4588 (1979).
[18]G. G. Ohlsen and P. W. Keaton, Nucl. Instrum. Methods 109, 41 (1973).
[19]J. F. Amann *et al.*, IEEE Trans. Nucl. Sci. NS-26, 4389 (1979).
[20]H. A. Bethe, Phys. Rev. 89, 1256 (1953).
[21]E. V. Hungerford *et al.*, Nucl. Phys. A197, 515 (1972).
[22]V. L. Highland, Nucl. Instrum. Methods 129, 497 (1975).
[23]A. M. Cormack, Nucl. Phys. 52, 286 (1964).
[24]G. Bendiscioli, E. Lodi Rizzini, and A. Rotondi, Nuovo Cimento 48A, 369 (1978).
[25]V. A. Andreev *et al.*, Leningrad Nuclear Physics Institute Report No. 656, 1980.
[26]M. W. McNaughton *et al.*, Phys. Rev. C 23, 1128 (1981).
[27]J. Bystricky *et al.* (private communication); F. Lehar, in *Proceedings of the International Symposium on High Energy Physics with Polarized Beams and Polarized Targets, Lausanne, 1980,* edited by C. Joseph and J. Soffer (Birkhauser, Basel, 1980), p. 319.
[28]R. A. Arndt *et al.*, *N-N* Computer Code, Virginia Polytechnic Institute, Solution SM80 (unpublished); R. A. Arndt, in *Polarization Phenomena in Nuclear Physics—1980 (Fifth International Symposium, Santa Fe),* Proceedings of the Fifth International Symposium on Polarization Phenomena in Nuclear Physics, AIP Conf. Proc. No. 69, edited by G. G. Ohlson, R. E. Brown, N. Jarmie, M. W. McNaughton, and G. M. Hale (AIP, New York, 1981).
[29]N. Hoshizaki, Prog. Theor. Phys. 61, 129 (1979).
[30]N. H. Buttimore, Phys. Rev. D 18, 694 (1978).
[31]C. Lechanoine, F. Lehar, F. Perrot, and P. Winternitz, Nuovo Cimento 56A, 201 (1980).
[32]H. G. Sharafnova, Fiz. Elem. Chastits At. Yadra 5, 645 (1974) [Sov. J. Part. Nucl. 5, 259 (1975)].
[33]H. A. Bethe, Ann. Phys. (NY) 3, 180 (1958).
[34]T. Lasinski, R. Levi Setti, B. Schwartzschild, and P. Ukleja, Nucl. Phys. B37, 1 (1972).
[35]W. Grein (private communication).
[36]C. Bourreley, J. Soffer, and D. Wray, Nucl. Phys. B77, 387 (1974).
[37]D. Aebischer *et al.*, Phys. Rev. D 13, 2478 (1976).
[38]J. D. Dowell *et al.*, Phys. Lett. 12, 252 (1964).
[39]L. S. Azhgirei and S. B. Nurushev, Zh. Eksp. Teor. Fiz. 45, 599 (1963) [Sov. Phys.—JETP 18, 412 (1964)].
[40]D. V. Bugg, in *Proceedings of the International Symposium on High Energy Physics with Polarized Beams and Polarized Targets, Lausanne, 1980,* edited by C. Joseph and J. Soffer (Birkhauser, Basel, 1980), p. 252; H. Spinka, Proceedings of the Workshop on Nuclear and Particle Physics at Energies up to 31 GeV: New and Future Aspects, Los Alamos, New Mexico, 1981, Los Alamos National Report Laboratory LA-8775-C, 1981, p. 220.
[41]D. V. Bugg, Nucl. Phys. A335, 171 (1980).